Towards a healthier workplace: how Flexos, an active and bilateral shoulder exoskeleton, provides support in weight-lifting and carrying tasks

Gianluca Rinaldi[1], Vladimiro Suglia[2], Luca Tiseni[3], Cristian Camardella[1], Michele Xiloyannis[4], Lorenzo Masia[5], Domenico Buongiorno[2], Vitoantonio Bevilacqua[2], Antonio Frisoli[1] and Domenico Chiaradia[1*]

***Abstract*—Work-related musculoskeletal disorders (WMDs) affect a high percentage of operators performing repeated weight lifting and load carrying in industrial scenarios. Since upper limb muscles are affected in the process, the assistance provided by upper body exoskeletons is increasingly needed to prevent WMDs and their consequent cost to the health system. This paper presents the evaluation of Flexos, a portable, bilateral, shoulder exoskeleton prototype designed to assist logistic and industrial operators in performing occupational tasks. An in-lab assessment was conducted on twelve healthy subjects - 9 males, 3 females - to evaluate Flexos capability in assisting the user during the execution of isometric, dynamic, and carrying-load tasks. Different metrics were extracted from time-series signals to assess the effort related to five targeted muscles surrounding the shoulder complex. Despite the limited experimental size and the prototypal level of the device, Flexos managed to cover almost all the shoulders range of motion - 89.2% flexion/extension, and 88.4% internal/external rotation - and to globally decrease muscular activity in occupational activities, particularly when isometric contractions are required for a prolonged time, with average reductions of -27.2% for the static task, -18.6% for the dynamic task and -23.4% for the carrying-load task.**

***Index Terms*—work-related musculoskeletal disorders, occupational exoskeletons, series-elastic actuators, assistive devices, active wearable robots, human-robot interaction (HRI), shoulder, muscular effort**

I. Introduction

High productivity requirements demanded by industrial and manufacturing scenarios force human operators to daily perform repetitive and exhausting actions with awkward body postures exposing them to injuries. This process, if excessively prolonged over time, may lead to medical conditions known as work-related musculoskeletal disorders (WMSDs). WMSDs are the first cause of occupational diseases in industrialized countries: they account for 15% of total healthcare costs in the EU-28, affecting the 60% workers and concurring in billions of dollars of lost production for the industry sector [1]. Since WMSDs mostly concern neck, shoulders, and back [2], the demand for direct upper body assistance in the workplace has been increasing in the past years.

Fig. 1. The proposed Flexos exoskeleton for the shoulder.

A major asset for the prevention of WMSDs in such complex environments is provided by occupational exoskeletons (OEs) designed for upper limbs. By means of actuation systems, these exoskeletons are able to provide torque to the user's arms, thus sustaining the upper limbs and relieving the local musculature during shoulder flexion/extension and weight lifting movements [3]. Industrial and logistic companies have increasingly shown interest in deploying OEs inside the workplace [4], with long-term expectations of reducing the occurrence of WMSDs and hence improving the related productivity of the human workforce by decreasing absence rate [5]. Moreover, the use of OEs has been demonstrated to reduce the required energy expenditure for completing a series of tasks, concurring in an overall redistribution of the latter among a reduced number of workers and thus resulting in a general decrease in costs [6].

Depending on their design, OEs for the upper body parts can be rigid [7] or soft [8]. A rigid device is characterized by the presence of a kinematic chain made of rigid links and linear/rotary joints, which act in parallel to the human upper limbs. These devices often struggle with joint misalignments, arising at the interfaces between human and robotic

[1] Gianluca Rinaldi, Antonio Frisoli, and Domenico Chiaradia are with the Institute of Mechanical Intelligence and the Department of Excellence in Robotics & AI, Scuola Superiore Sant'Anna, Pisa, Italy.

[2] Vladimiro Suglia, Domenico Buongiorno, and Vitoantonio Bevilacqua are with the Department of Electrical and Information Engineering (DEI), Polytechnic University of Bari, 70126 Bari, Italy.

[3] Luca Tiseni is with the Next Generation Robotics Srl, Pisa, 56123, Italy.

[4] Michele Xiloyannis is with the Akina AG, Zürich, 8005, Switzerland.

[5] Lorenzo Masia is with the Munich Institute of Robotics and Machine Intelligence (MIRMI), Technische Universität München (TUM), 80992, Munich, Germany.

* corresponding author: domenico.chiaradia@santannapisa.it

joints. These issues become challenging particularly when dealing with the shoulder complex, consisting of a total of 5 Degrees Of Freedom (DOF). On the opposite side, a soft exoskeleton only consists of wearable garments equipped with soft actuation systems, such as cable tendons or pneumatic muscles. These devices tend to be lightweight and capable of preventing discomforts caused by joint misalignments since they do not feature a kinematic chain [9]. However, employing soft garments, which are characterized by specific structural performances, prevents these devices from providing more than a limited amount of torque [10]. So far, this issue has strongly limited the use of soft exoskeletons in industrial scenarios [11].

Another crucial factor involves the exoskeleton actuation system, where predominant solutions to date mainly rely on passive energy storage systems, such as springs [12]–[15]. Despite being extremely light and simple, these devices do not provide real-time adjustable torque, as their estimates only depend on the shoulder flexion/extension angle and fixed design parameters, such as the selected spring stiffness. On the contrary, active solutions can provide any desired amount of torque at any time, since they are usually based on electric motors whose limitations are only related to their structural configuration and absorbed power [16]. A great design candidate for active systems is provided by Series Elastic Actuators (SEAs), which offer an estimation of the interaction torque by measuring the angular displacement of the series elastic joint. This facilitates the retrieving of feedback torque data, enabling real-time closed-loop torque control and thereby ensuring safety in physical Human-Robot Interaction (pHRI) [17].

Additionally, active systems facilitate the integration of assistance strategies driven by intelligent algorithms that draw insights from data of various types, such as signals related to inertial measurement units (IMUs) or muscular activities measured with electromyography (EMG) sensors [18]. However, these systems are frequently more complex and bulkier if compared to their passive counterparts [19]. For this reason, minimizing the number of active joints could provide a good compromise between the higher controllability of active exoskeletons and the device's ergonomics.

Lastly, since the in-lab validation of an OE is the first step in the path towards a larger adoption of the device, the design of the experimental protocol becomes relevant. An efficient protocol must be capable of representing both biomechanical effects on the users' physical effort as well as potentially undesired effects [5]. To the authors' knowledge, the majority of portable upper-limb exoskeletons for workers underwent an in-lab assessment mainly based on static tasks either over the head [20]–[22] or under the head [23]. There are some minor exceptions featuring the dynamic lifting [24] and carrying of loads of various weights [25], [26]; nonetheless, passive devices are mostly employed in these cases.

In light of the above-mentioned works, an interesting gap has been noticed in the literature regarding both the design of active OEs to support humans in lifting weights and their in-lab assessment through static and dynamic tasks resembling daily occupational activities. This paper presents the evaluation of Flexos, a completely portable, lightweight - $8\,\mathrm{kg}$, battery included - and series-elastic actuated shoulder exoskeleton. *The main contribution* consist in:

1) demonstrating how Flexos, despite having a very simple design providing only one actuated degree of freedom, is capable of reducing the muscular effort of shoulder complex muscles to a comparable extent with respect to similar prototypes;
2) assessing Flexos efficacy during complex occupational tasks involving the lifting and carrying of objects.

This work extends the preliminary research conducted on Flexos [27] by including a bilateral design, which not only enables full assistance on both arms at the same time but also provides a more uniform redistribution of the exoskeleton weight throughout the user's body, thus favoring comfort and general performances. Moreover, the torque controller is updated for the user's intention awareness by taking into account the arm speed as a feedforward component inside the controller itself. Additionally, the experiment protocol is improved to be more closely inspired by occupational scenarios: a set of static and dynamic experiments on twelve healthy subjects, involving the lifting, carrying, and shelving of two different weights - $3\,\mathrm{kg}$ and $5\,\mathrm{kg}$ - at different heights is proposed to assess Flexos' contribution in reducing the user's muscular effort. These new experiments provide a more thorough analysis of the biomechanical benefits of employing an active OE for daily occupational tasks.

The outline of this article is organized as follows: Section II describes the mechanical design and the control system of the proposed device; Section III explains the experiments conducted for evaluating Flexos assistive efficacy; the outcomes of the data analysis carried out for this latter validation are provided and discussed in Section IV; ultimately, Section V contains the drawn conclusions about the study and the ideas for future works.

II. System Description

A. Mechanical design

Flexos main subsystems are shown in Fig. 2 (a) and its kinematics, together with the human one and their connection, is shown in Fig. 2 (c). Since most of Flexos custom-made rigid parts are produced using 3D printing technology, with additional soft interfaces that are hand-sewn to the rigid surfaces, the whole system is still considered a prototype.

The device interfaces with the human body through both a primary rigid part located at the back - Fig. 2 (a), 2 - and one arm interface - Fig. 2 (a), 4 - for each side, attachable around the upper limbs using two Velcro strap bands. A kinematic chain - Fig. 2 (a) - links the two primary human-robot interfaces (back and arm) together. One extremity is fixed to the back interface, while the other one is connected to the SEA - Fig. 2 (a), 3 - hosting the motor (T-Motor AK80-9). Employing the SEA for Flexos not only helps decouple the motor side from the link side of the exoskeleton, thus protecting both the human from any electrical instabilities and the motor from possible impacts at the end-effector of the device, but it provides the Flexos controller with the torque information it needs to close the control loop. The

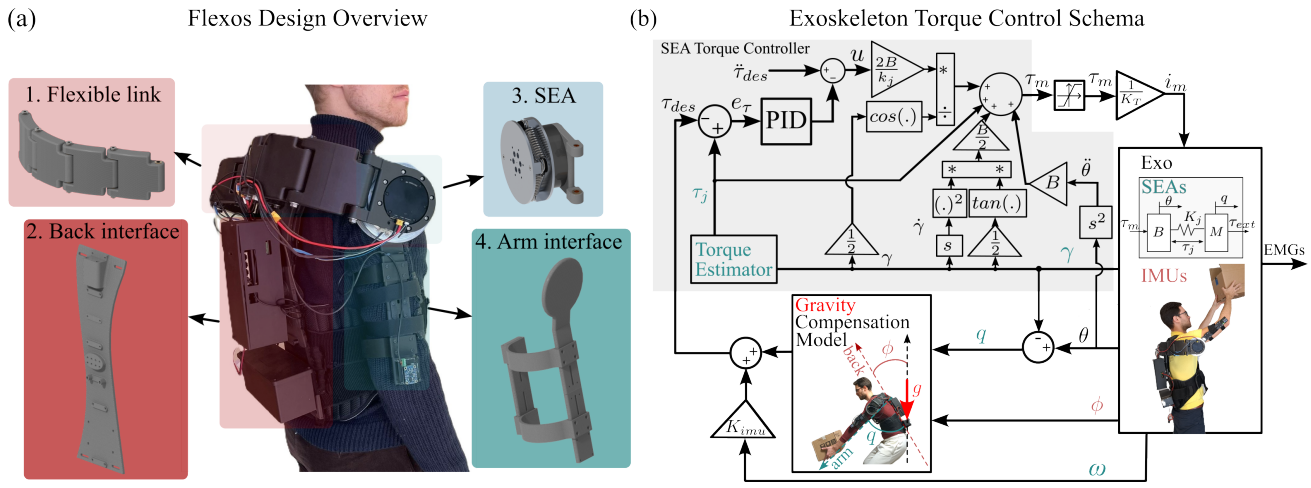

Fig. 2. (a) Flexos design overview. (b) Exoskeleton torque control schematic diagram. The gray part of the schema refers to the SEA torque controller.

kinematic chain of the exoskeleton is not compatible with the typical abduction/adduction motion performed with the arms positioned alongside the body. This choice, although not ideal, is task-oriented and finalized at improving the device weight and robustness as much as limiting controller complexity: a possible solution would be, in fact, the addition of a second motor to properly perform the abduction/adduction motion, resulting in an overall increasing of system complexity. To bypass the issue, the user is now allowed to reach a comparable posture by combining the other compatible movements of flexion/extension and internal/external rotation.

B. Control & communication systems

All essential components for control and communication are housed inside a box that is embedded in Flexos backpack, making the device completely portable. The main control unit of the system is represented by a Teensy 4.1 board which communicates via UDP with an external host-PC that is used to change internal settings.

The microcontroller is integrated into a printed circuit board (PCB) that hosts all the connectors for power, sensors, and actuators, it operates at a rate of 1 KHz and handles the communication with the motors (CAN), the IMUs (I2C) and the encoders (SSI) embedded in SEA to measure the angular displacement of the elastic joint. There are three BNO055 IMU boards mounted on Flexos: the first one is placed on the back interface and serves as the main reference for the other two IMUs that are located on each arm interface and measure the arms' Euler angles and angular velocities.

The external host-PC operates at a 500 Hz and can dynamically adjust control parameters (e.g., maximum desired torque, control gains, and operating mode) while also retrieving all the relevant data gathered by the Teensy board.

Lastly, the back interface also hosts the power storage system - a 24 V, 10 Ah LiFePO4 battery weighing 1.4 kg. The system is capable of being powered on continuously for 44 h when the motors are powered off, for 11 h when both the motors exert a fixed 5 Nm torque, and for 16 h when the motors exert 5 Nm of torque with a 50% duty cycle.

TABLE I
CONTROL PARAMETERS

Parameter	Value
Joint stiffness k_j	72.4 Nm/rad
Motor torque constant K_T	0.945 Nm/A
Max. system output torque τ_{max}^{system}	9 Nm rated, 18 Nm max
Max. gravity contribution torque $\tau_{max}^{gravity}$	5 Nm
Proportional gain K_p	1.5
Derivative gain K_v	0.015 s
Integral gain K_i	0.50 s^{-1}
Velocity-dependent torque gain K_{imu}	0.002 Nm $*$ s/rad

C. Torque controller

Fig. 2 (b) shows Flexos' torque controller scheme, whose goal is to partially compensate for the gravity torque that arises from the arm weight - either alone or eventually with a lifted object - during the shoulder flexion/extension. However, the maximum torque due to gravity compensation $\tau_{max}^{gravity}$ provided by the exoskeleton is limited in the controller at 5 Nm, since previous experimental evaluations revealed that higher torque values could lead to localized deformations in the 3D-printed parts the current Flexos version uses, particularly when shoulder flexion is at 90 ° and flexion speed is almost zero. Such deformations could compromise the structural integrity of the device and, consequently, its performance in assisting the user.

The SEA provides an estimate of the joint torque based on Hook's law and expresses the proportional relationship between the elastic torque τ_j exerted through the linear springs of the SEA and the angular displacement of the joint γ, with the first-order joint stiffness k_j experimentally evaluated in [28] and reported in Tab. I. The join torque is equal to:

$$\tau_j = k_j \sin\left(\frac{\gamma}{2}\right) \tag{1}$$

The SEA torque controller follows the method of [29], adapted to the nonlinear joint under study. The dynamic

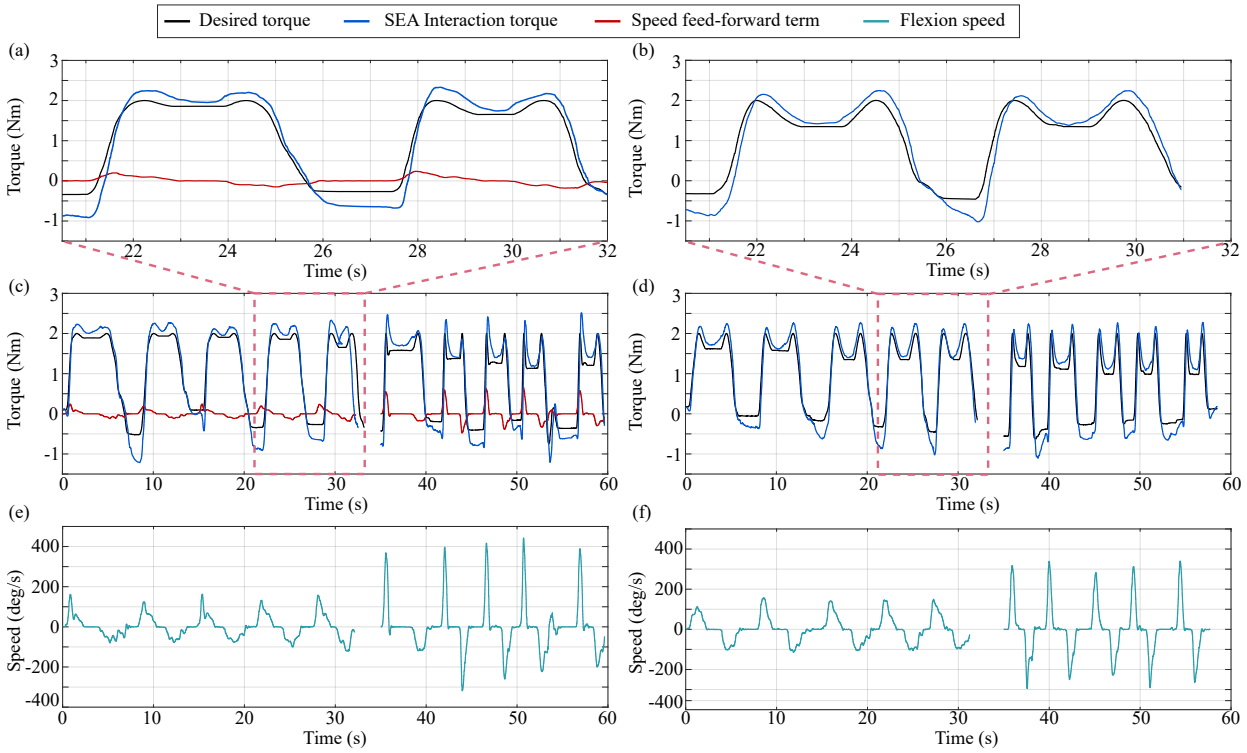

Fig. 3. Comparison of the torques and speed profiles when using the interaction controller with the speed-dependent feed-forward term (a),(c), and (e), and without the feed-forward term (b), (d), and (f). From a comparison between the SEA closed-loop interaction forces in the two conditions (a) and (b), it can observed that the speed-dependent feed-forward term led to reduce the tracking delay, from around 100 ms to 45 ms. The time delay has been computed by averaging the delays between the two times to peak.

equations of the SEA system in Fig. 2(b) are:

$$\begin{aligned} B\ddot{\theta} &= \tau_m - \tau_j \\ M\ddot{q} &= \tau_j + \tau_{ext} \end{aligned} \tag{2}$$

where B and M represent the motor-side and link-side inertia, respectively; θ and q represent motor and link angular position, τ_m is the torque applied to the elastic joint by the motor, τ_j is the torque applied by the joint to the link, and τ_{ext} is the interaction torque applied to the link.

The magnetic encoder provides the elastic joint's angular displacement γ, computed as:

$$\gamma = \theta - q \tag{3}$$

To determine the interaction between motor torque and joint torque dynamics, the second time derivative of Eq. 1 is computed and, using Eq. 3, the following equation is obtained:

$$\ddot{\tau_j} = \frac{k_j}{2}\left(\ddot{\theta} - \ddot{q}\right)\cos\left(\frac{\gamma}{2}\right) - \frac{k_j}{4}\dot{\gamma}^2 \sin\left(\frac{\gamma}{2}\right) \tag{4}$$

By substituting the first of the dynamic Eqns. 2, the motor torque appears in the joint torque dynamics.

$$\ddot{\tau_j} = \frac{k_j}{2}\left(\frac{\tau_m - \tau_j}{B} - \ddot{q}\right)\cos\left(\frac{\gamma}{2}\right) - \frac{k_j}{4}\dot{\gamma}^2 \sin\left(\frac{\gamma}{2}\right) \tag{5}$$

Although the system dynamics are nonlinear, the motor torque τ_m can be suitably selected to cancel these nonlinear effects while incorporating a feedback control law u:

$$\tau_m = \tau_j + B\ddot{q} + \frac{B}{2}\dot{\gamma}^2 \tan\left(\frac{\gamma}{2}\right) + \frac{2\,B}{k_j\,\cos\left(\frac{\gamma}{2}\right)}u \tag{6}$$

Combining Eqns. 5 and 6 the joint torque dynamics reduces to:

$$\ddot{\tau_j} = u \tag{7}$$

According to [29], a simple feedback control law for SEA rejecting disturbances and leading to a stable error dynamics is a PID controller that can be defined as:

$$u = \ddot{\tau}_{des} - (K_v\,\dot{e_\tau} + K_p\,e_\tau + K_i \int e_\tau) \tag{8}$$

where τ_{des} is desired torque and the error e_τ is defined as:

$$e_\tau = \tau_j - \tau_{des} \tag{9}$$

PID controller gains are tuned with the Ziegler-Nichols method and reported in Tab. I. The resulting motor torque command τ_m is converted into a current value and sent to the motors.

The desired torque reference τ_{des} for the closed-loop controller is obtained by the Gravity Compensation Model plus an additional velocity-dependent torque contribution as shown in Eqn. 10:

$$\tau_{des} = \tau_{max}^{gravity}\,\sin\left(q - \phi\right) + K_{imu}\,\omega \tag{10}$$

where $\tau_{max}^{gravity}$ represents the maximum torque value for the gravity contribution term, and q is the flexion/extension angle of the shoulder - the link side angle of the SEA - The IMU located on the back interface measures the misalignment between its vertical axis - parallel to the user's back plane and thus to the longitudinal axis - and Earth's gravity vector.

The resulting angle ϕ is subtracted to q and the obtained assistance becomes proportional to the difference between the two antagonist angles, as reported in Eqn. 10. Additionally, the desired torque reference τ_{des} is proportional to the shoulder flexion speed ω, which is measured by the IMUs located on each arm interface and then scaled by a constant value K_{imu}. By taking into account the flexion/extensions angular speed, the authors aim to provide an additional contribution to the controller reference generation that takes into account the user's intentions.The K_{imu} value is tuned with the purpose of keeping the velocity-dependent torque contribution peaks at $1\,\mathrm{Nm}$ maximum, since this was the value that was empirically demonstrated to provide a perceived improved assistance for the user.

Fig. 3 shows the results of some qualitative tests conducted on 5 subjects to assess the benefits of this feed-forward, velocity-dependent component. Subjects were instructed to perform some weight lifting movements, involving shoulder flexions from $0\,^\circ$ to $90\,^\circ$ and extension from $90\,^\circ$ to $0\,^\circ$, without imposing any time or velocity limitations. A delay reduction between the desired torque and the controlled interaction torque from the SEA is evident in Figures 3 (a) and (b). This delay passed from around $100\,\mathrm{ms}$ to $45\,\mathrm{ms}$. The greater delay of the controller without the compensation term led to a more oscillatory behavior of the joint when the user was going to stop his/her motion. This difference is more perceivable at lower speeds - under $200\,^\circ/\mathrm{s}$. In the case of medium-high speed - from $300\,^\circ/\mathrm{s}$ to $500\,^\circ/\mathrm{s}$ - the beneficial effect of a lower delay is partially masked from the additional torque contribution, resulting in an overcompensation when the subject suddenly tries to stop his/her movement - K_{imu} was tuned accordingly.

D. Biological and assistive torque considerations

The partial assistance of $5\,\mathrm{Nm}$ can be expressed as a percentage of relief from the human arm, or human arm plus load weight. To frame the impact of the $5\,\mathrm{Nm}$ provided by the exoskeleton to the human shoulder joint, we can use a simplified planar schema of the human arm in the sagittal plane that considers the shoulder, elbow, and wrist flexion joint as rotoidal joint and the arm, forearm, and hand as link in two configurations/scenarios (see Figure II-D). For the mass distribution and lengths of the human arm parts, we referred to [30], which evaluates the masses and lengths as a percentage of the body weight and stature, respectively. This led to results reported in Table II. For simplicity, we assume the center of mass of each body segment is half its length, except for the hand, which is set to a third of its total length. For the external load, we use the equivalent of $5\,\%$ of the body weight. In the case of an isometric task, $5\,\mathrm{Nm}$ of assistance corresponds to a $45.01\,\%$ of arm weight relief, whereas it is equal to $14.15\,\%$ of arm+load weight relief. In another relevant use case scenario, that is the overhead task - i.e. the external load is hold with both shoulder and elbow flexion angles equal to $90\,^\circ$ -, the percentages of assistance are higher: $62.84\,\%$ of arm weight relief, and $25.71\,\%$ of arm+load weight relief. Absolute and relative values of the torques are reported in Table III.

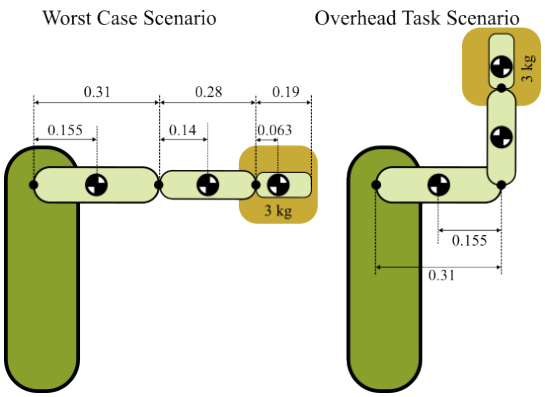

Fig. 4. Simplified schema of human body in the two selected scenarios to evaluate the impact of the assistive torque on the shoulder flexion joint.

TABLE II
MASS AND LENGTH OF THE ARM, FOREARM, HAND, AND EXTERNAL LOAD.

Body link	% Body Weight	Weight (Kg)	% Stature	Length (m)
Body	100	75	100	1.80
Arm	2.64	1.98	17.35	0.31
Forearm	1.531	1.15	15.72	0.28
Hand	0.612	0.46	10.54	0.19
Ext. load	5	3.75	-	-

TABLE III
BIOLOGICAL TORQUE IN THE WORST CASE AND OVERHEAD TASK SCENARIOS.

Torques	Worst Case	Overhead Task
τ_{bio} (Nm)	11.11	7.96
$\tau_{bio+load}$ (Nm)	35.33	20.38
τ_{assist}/τ_{bio} (%)	45.01	62.84
$\tau_{assist}/\tau_{bio+load}$ (%)	14.15	25.71

III. EXPERIMENTS

A. Participants

A series of in-lab experiments were performed on twelve healthy subjects (28.00 ± 2.08 years old, height $183.4 \pm 3.1\,\mathrm{cm}$, BMI $23.14 \pm 1.82\,\mathrm{kg/m^2}$), with only one left-handed, with neither previous history of neuromotor disorders nor a former familiarity with occupational exoskeletons. The experimental protocol conformed to the ethical standards laid down in the 1964 Declaration of Helsinki. Ethical approval for the study was granted by the Scuola Superiore Sant'Anna Review Board, ID 152021, and the written informed consent was obtained from each participant prior to the experiments.

B. Experimental Setup

The in-lab assessment of Flexos aims to evaluate how effectively the exoskeleton supports the user during repeated upper-limb elevation tasks by both measuring achievable ROM, tracking arm movements within the workspace, and assessing reductions in perceived exertion and muscular effort.

ROM is computed through the IMUs located on each arm interface, which are also used for motion tracking together with a virtual reality tracking system [31]. This latter consists

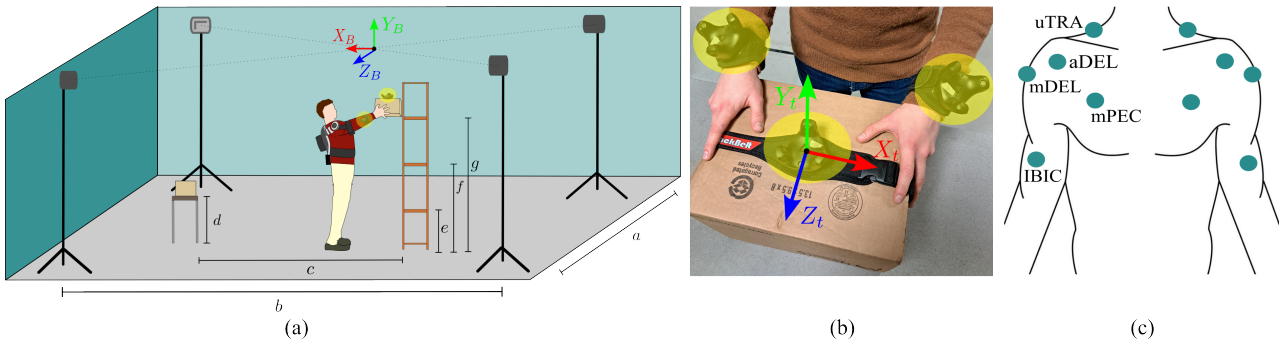

Fig. 5. Experimental setup. The room for the experiments is shown in (a): the subject's motion path includes a starting platform where the package is lifted from and a final shelving unit where the package is shelved. Three different shelf heights, which are labeled as e, f, and g, are encompassed in this experiment. The base stations are located at the four corners of the room such that there is no occlusion among them and each marker is always tracked by at least two base stations. The base stations generate an absolute coordinates system $(XYZ)_B$ that serves as a reference for the individual coordinates system $(XYZ)_t$ of the three used trackers (b). One tracker is positioned at the top-center of the box, whereas the other two trackers are located at the user's wrists. (c) EMG Trigno sensor positioning. Each sensor is located along the longitudinal midline of each targeted muscle, thus the sensor midline is parallel to the muscle fiber direction.

of four HTC SteamVR Base Station 2.0, located at the four corners of the experiments room (Fig. 5 a), and three VIVE Tracker 3.0, two of which are positioned on each subject's wrist and the third of which is located on the target box (Fig. 5 b). Trackers and base stations are managed by SteamVR which acquires linear and angular positions and speeds at 250 Hz.

Muscular effort evaluation involves measuring the electromyography (EMG) activity of five specific muscles - biceps brachii (lBIC), anterior deltoid (aDEL), medial deltoid (mDEL), pectoralis major (mPEC), and upper trapezius (uTRA) - during the experiments tasks, each one repeated in two different conditions: with (w. Exo) and without (w.o. Exo) the exoskeleton worn and powered on. EMG signals have been recorded using a Trigno Wireless Biofeedback System (Delsys, Natick Massachusetts, USA), which comprises a main base station and two types of wireless EMG sensors - Trigno Avanti and Trigno Quattro EMG Sensors - as shown in Fig. 5 (c). Each targeted muscle is monitored with one EMG sensor unit carefully placed by following the SENIAM recommendations [32]. A Delsys Trigger Module is used for synchronizing the EMG data with the trackers and exoskeletons data, acquired by the main control unit. The recorded data are then exported and processed using MATLAB. The raw EMG data undergoes band-pass filtering (35-450 Hz), full-wave rectification, and a low-pass filtering (6 Hz) via a zero-phase second-order Butterworth filter. The EMG activity is then normalized using the maximum voluntary contraction (MVC) value of each different subject. Furthermore, EMG signals have been segmented by taking the linear position of the object as a visual reference.

C. Experimental Protocol

Flexos experimental protocol, inspired by occupational scenarios, is based on four main tasks, structured as follows:

- **Range of Motion (ROM) task**: the participant is instructed to perform free movements of shoulder flexion/extension, internal/external rotation, and a combination of the two motions to obtain the abduction/adduction. The participant is asked to perform each movement trying to reach the maximum limit of the shoulder range of motion in his/her capabilities.
- **Isometric task**: the participant is asked to hold a box with both hands while keeping both arms elevated - horizontal, at 90 ° elevation on the sagittal plane (with a tolerance of ±3 °) - until either voluntary exhaustion [33] or for a maximum of 2 minutes. Note that corrective feedback has been provided by the experimenter when the subject's shoulder flexion angle became lower than 87 ° or higher than 93 °.
- **Dynamic task**: each participant is asked to stay at a reference distance of 70 cm from a shelving unit that is made up of three shelves in total. The task is divided into two main motor actions, combined together to form a whole trial.
  1) *Upwards motion*: The participant is instructed to grab with both hands a box located at the *middle* shelf and shelve it onto the *top* shelf; then, the subject brings both arms back in the resting position - parallel to the trunk.
  2) *Downwards motion*: The participant grabs with both hands the box, now located at the *top* shelf, and shelves it back onto the *middle* shelf. After that, the subject brings both arms to the resting position.

  Each transition - up, down, rest - is performed between two consecutive beats of a metronome set at 20 bpm. The task is performed for a maximum of 2 minutes.
- **Carrying-Load task**: This task is inspired by the ex-

TABLE IV
EXPERIMENTS - ROOM DIMENSIONS AND DISTANCES

Parameter		Value [m]
Distance between base stations ⊥ path	a	5.70
Distance between base stations // path	b	8.60
Path length	c	3.20
Starting table height	d	0.82
Shelving unit, *lower* shelf height	e	0.69
Shelving unit, *middle* shelf height	f	1.20
Shelving unit, *top* shelf height	g	1.59

This article has been accepted for publication in IEEE Transactions on Robotics. This is the author's version which has not been fully edited and content may change prior to final publication. Citation information: DOI 10.1109/TRO.2026.3666155

(a) (b) (c) (d)

Fig. 6. The three phases of the Carrying-Load Task. (a)-(b) *Pickup*, (c) *Carrying*, (d) *Release*.

periments of Theurel et al. [25], and it mostly features movements with shoulders flexed at $90\,^{\circ}$, where the gravity torque is maximum, thus this posture is ideal to test the maximum assistive effect of the exoskeleton in the worst case. This task is divided into three main motor actions as shown in Fig. 6.

1) *Pickup*: The participant is asked to stand in front of the table where the box is located, then grab the box with both hands and lift it, performing a shoulder flexion movement until the arm reaches $90\,^{\circ}$ on the sagittal plane.
2) *Carrying*: The participant turns around and walks towards the shelving unit on the opposite side. While walking, the subject keeps carrying the box with arms at $90\,^{\circ}$ elevation on the sagittal plane. The participant is asked to synchronize each step with the beat coming from a metronome set at $80\,\mathrm{bpm}$.
3) *Release*: The participant reaches the shelving unit and leaves the box on one of the three shelves.

The three actions are then repeated in the opposite direction, with each subject lifting the box from the shelving unit and carrying it back to the starting table, thus completing a whole trial. At each subsequent cycle, the subject is asked to shelve the box in a different layer of the shelving unit (in order, *middle*, *top*, *middle*, *lower*). The metronome also supports an additional paced action: each phase is preceded by a brief pause where the subject is requested to stand still while holding the box for three consecutive beats. This will help identify motor actions while inspecting signals in post-processing. The whole task is executed until voluntary exhaustion or for a maximum of 10 minutes.

Every task has been repeated both with Exo (w. Exo) - torque controller powered on - and without (w.o. Exo). For every subject, one condition (w. or w.o. Exo) is randomly selected at first, and for each condition all the tasks are executed in sequence. The order of execution of the tasks for each condition has been randomized to be different for each participant. Only the ROM task is not randomized and always executed before both conditions, since it is only performed w. Exo but with torque controller powered off.

The shelving unit used in the dynamic and carrying-load tasks is the same for all subjects. Its characteristics are depicted in Fig. 5 (a) and numerically reported in Table IV. The authors are aware that such parameters should have been tailored to the subject's anthropometric characteristics (height, arm length) for the sake of a fair comparison. However, it has not been modified since the inter-subject variability in terms of height - reported in Subsection III-A - is low.

Isometric and dynamic tasks are performed twice, each time with a box of different masses - $3\,\mathrm{kg}$ and $5\,\mathrm{kg}$ -. The order of masses is pseudo-randomized each time. The carrying load task is only performed with the $3\,\mathrm{kg}$ box, in order to prevent the subject from excessive fatigue since this task is the longest one.

The participant is required to rest for a minimum of ten minutes between two subsequent executions of each task, to allow muscle relaxation before proceeding to the next task, thus preventing fatigue from altering the results. The maximum duration of dynamic and carrying-load tasks was chosen to both optimize the global experimental time and attempt to acquire a sufficient amount of data to assess the influence of the exoskeleton [34].

After each task, to collect a qualitative assessment of the task load, the participants filled the 20-point scale NASA Task Load Index (NASA-TLX) questionnaire made up of 6 items, mental demand (MD), physical demand (PD), temporal demand (TD), performance (P), effort (E), and frustration (F) [35]. In addition, the Borg CR-10 [36] questionnaire has been included to qualitatively evaluate the rate of perceived exertion (RPE) as well.

D. Metrics and statistical analysis

Different metrics have been extracted from the processed data in both w. and w.o. Exo conditions to quantitatively assess Flexos' assistance.

- **Endurance time**: the ET is the duration of the isometric task, computed as the time elapsed from the first to the last instant in which the subject kept the shoulder flexed at $90\,^{\circ}$.

- **Muscular effort**: the ME is computed as the root mean squared (RMS) of each processed EMG signal. Since subjects could reach fatigue at different times w. Exo and w.o. Exo, the ME values may be biased from a delay of the fatigue onset. Hence, for the sake of a fair comparison, the minimum time between the w.o. Exo and w. Exo conditions have been considered for each task. Then, the RMS is computed for each targeted muscles over the length of the whole signal for the isometric task, and within all the phases or subphases of the dynamic and carrying-load tasks, respectively. The intra-subject mean of the ME has been computed for the dynamic and carrying-load tasks.
- **Qualitative feedback**: NASA-TLX and Rate of Perceived Exertion (RPE) indexes are evaluated from questionnaires provided to each subject after completing all the tasks related to a single condition (either w. Exo or w.o. Exo).

For all the metrics, an inter-subject median is computed for every index. The percentage reductions are then computed as the relative difference between the inter-subject medians of the two main conditions (i.e., w.o. Exo and w. Exo). The normality distribution of all the metrics is checked by means of a Shapiro-Wilk test with a significance level of $\alpha = 0.05$. Consequently, the value of these metrics in the w. Exo condition is statistically compared with the one in the w.o. Exo condition through a non-parametric Wilcoxon signed-rank test for non-normally distributed sets and with a paired t-test ($\alpha = 0.05$) for normally distributed ones. In doing so, the possible statistical significance of any variations between the w. Exo and w.o. Exo conditions can be checked.

IV. Results & Discussion

A. ROM task

The outcome of the ROM task is determined by the Euler angles measured with the IMUs located on each arm interface. To assess the accuracy of IMU data, the inter-subject mean of the shoulder flexion angle of the isometric task is computed for both the $3\,\mathrm{kg}$ and $5\,\mathrm{kg}$ weights. The results is an accurate $88.73 \pm 2.4^\circ$ of shoulder flexion while isometrically holding the weight.

TABLE V
Shoulder ROM. Ground truth data for healthy subjects are taken from [37] and compared to the ROM covered with Flexos. Values are reported in mean ± standard deviation.

	w.o. Exo [37]	w. Exo
Flexion	$166.7^\circ \pm 4.7^\circ$	$149.2^\circ \pm 9.24^\circ$
Extension	$62.3^\circ \pm 9.5^\circ$	$55.1^\circ \pm 9.0^\circ$
Internal Rot.	$68.8^\circ \pm 4.6^\circ$	$66.7^\circ \pm 4.9^\circ$
External Rot.	$103.7^\circ \pm 8.5^\circ$	$85.7^\circ \pm 3.4^\circ$

The kinematic model for ROM measurements is compliant with the Thorax coordinate system recommended by the International Society of Biomechanics (ISB) [38]. Table V presents the results for shoulder flexion/extension and internal/external rotation. To ensure consistency with the literature, these results are compared with the normal values of forward flexion, backward extension, and inward/outward rotation stated by Boone et al. (1979) [37]. The results show how Flexos allows extensive coverage of human ROM, achieving an average of 89.2% for flexion/extension motion and 88.4% for internal/external rotation.

Since the presence of the exoskeleton does not prevent the wearer from covering most of the shoulder ROM, participants did not complain about the impossibility of performing a direct shoulder abduction/adduction motion when the arm is placed along the body, as they easily used the other available DOFs.

B. Isometric task

Fig. 7 shows the outcomes of the isometric task. Although not statistically significant, the endurance time (Fig. 7b) in the w. Exo condition is higher than in the w.o. Exo condition for both masses. This suggests that the exoskeleton effectively increased the subject's endurance during the isometric task.

The distributions of the muscular effort during the isometric task for all the subjects are reported in Fig. 7 (a). The median of the ME during the isometric task in the w. Exo condition is lower than the one in the w.o. Exo condition in almost

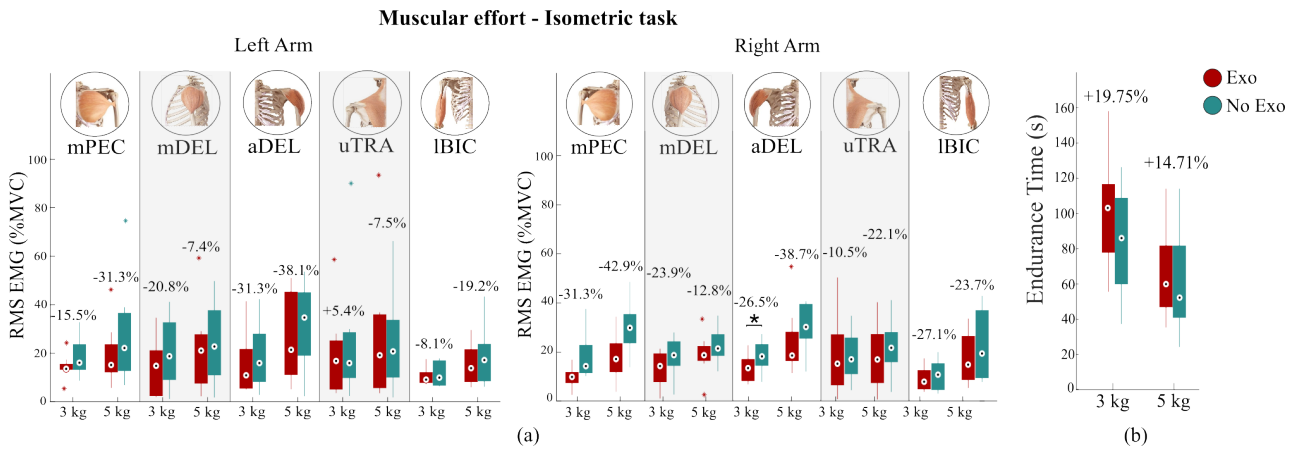

Fig. 7. (a) RMS during isometric task. Percentage differences in RMS between w. Exo and w.o. Exo conditions are reported, with * representing statistically significant comparisons with $p < .05$. (b) Endurance time during isometric task.

This article has been accepted for publication in IEEE Transactions on Robotics. This is the author's version which has not been fully edited and content may change prior to final publication. Citation information: DOI 10.1109/TRO.2026.3666155

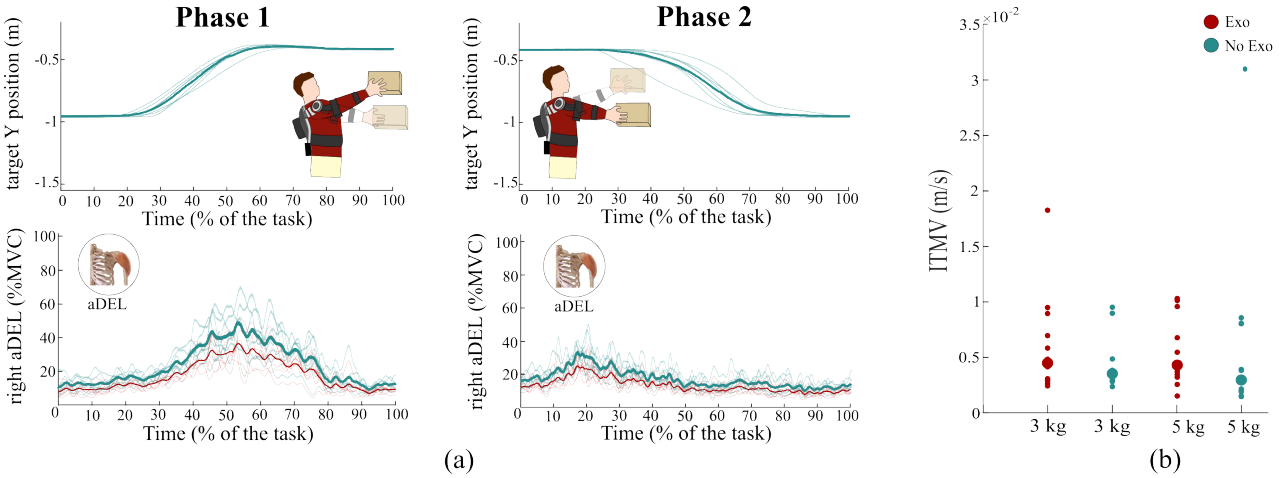

Fig. 8. (a) Position of the target box and muscular activation of the right anterior deltoid during the dynamic task executed with the 3 kg box. The thicker colored lines represent the inter-trial mean among corresponding signals, for both Exo and No Exo conditions; the other, shaded lines are related to single trials. Data refer to one representative subject. (b) Inter-trial mean velocity during the dynamic task.

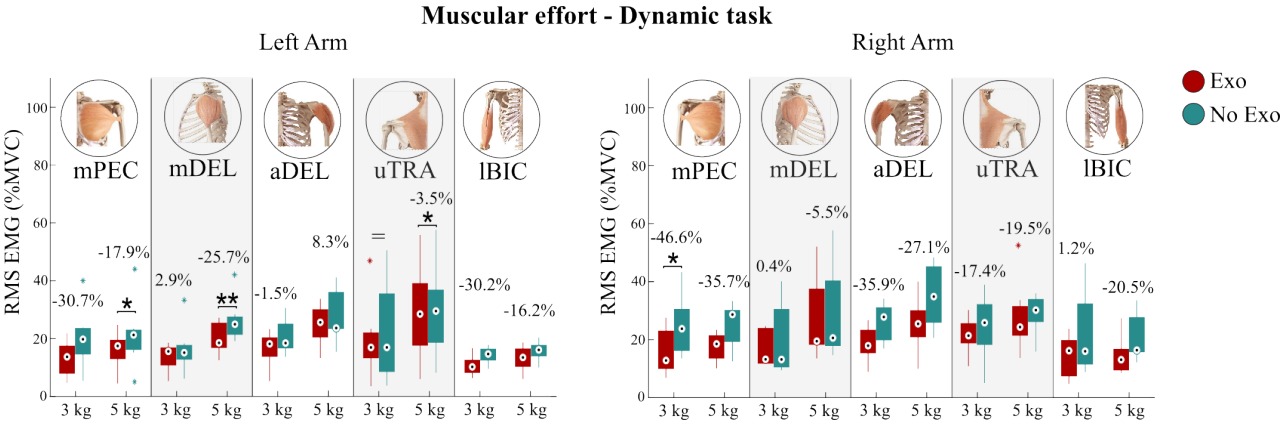

Fig. 9. RMS during dynamic task, with * and ** representing statistically significant comparisons with $p < .05$ and $p < .01$, respectively. Percentage differences in RMS between w. Exo and w.o. Exo conditions are reported. The = marks no reduction nor increase in the related index.

all cases, with statistical significance for the right aDEL (-26.5%, p=0.013). No muscle targeted by the robotic assistance was penalized by the introduction of Flexos. Therefore, the ME values assess the benefits of employing an occupational exoskeleton for shoulder assistance in isometric tasks.

C. Dynamic task

Fig. 8 and Fig. 9 show the outcomes of the dynamic task. Considering a representative subject of the collected dataset performing the task with the 3 kg box, Fig. 8 (a) shows the temporal evolution of the vertical position of the object that is moved upwards (i.e., from the middle to the upper shelf) and downwards (i.e., from the upper to the middle shelf) in the dynamic task, using the reference system that is shown in Fig. 5 (a). Moreover, the processed EMG signal of the right aDEL is shown, reflecting the corresponding muscular activation. For both signals, the inter-trial mean has been included, and the time axis has been normalized. Both phases (upwards and downwards motions) can be divided into three subphases, which are: a) a reaching subphase that lasts 25% of the whole time cycle on average, b) a moving phase that lasts from the 25% to the 70% of the whole time cycle on average, and c) a release phase that lasts for the remaining 30% of the time cycle on average.

Moreover, the distribution of the inter-trial mean velocity (ITMV) was computed to demonstrate how each group of tasks was executed as much as possible at the same speed, to exclude the effect of movement speed on the effort evaluation. As shown in Fig. 8 (b), there is no substantial difference between the w. Exo and w.o. Exo conditions, highlighting how the velocity has not evidently changed during the dynamic task.

Concerning the ME, its distributions during the dynamic task for all the subjects are reported in Fig. 9. The median of ME during the dynamic task in the w. Exo condition is higher than that of the w.o. Exo condition only for the left aDEL, even though slightly and not statistically significant (+8.3%, p=0.395). Although this is a muscle directly involved in the task and primarily assisted by the exoskeleton, this increase could be the result of how the weight of the exoskeleton is left to be naturally managed by the user, who could have performed muscle contractions in an asymmetrical way. Statistically significant results concern the left uTRA (-3.5%,

This article has been accepted for publication in IEEE Transactions on Robotics. This is the author's version which has not been fully edited and content may change prior to final publication. Citation information: DOI 10.1109/TRO.2026.3666155

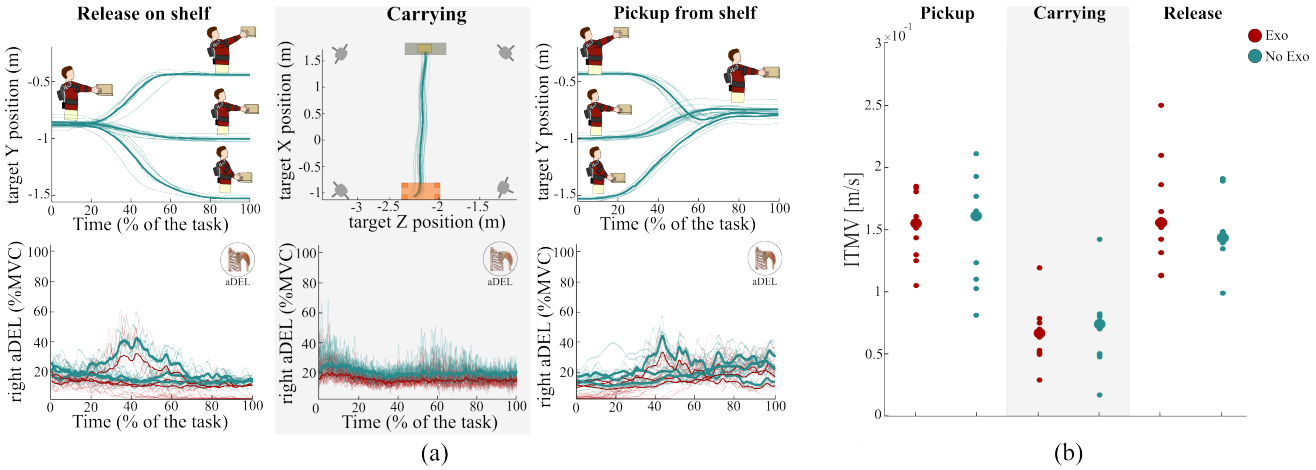

Fig. 10. (a) Position of the target box and muscular activation of the right anterior deltoid during the carrying-load task executed with the 3 kg box. The thicker colored lines represent the inter-trial mean among corresponding signals, for both Exo and No Exo conditions; the other, shaded lines are related to single trials. Data refer to one representative subject. (b) Inter-trial mean velocity during the carrying-load task.

p=0.0032), mDEL (-25.7%, p=0.006), and mPEC (-17.9%, p=0.034), as well as a consistent decrease for the right mDEL (-46.6%, p=0.023). Nonetheless, if compared to the isometric task, the percentage reductions in the dynamic task are overall slightly lower, particularly for the mDEL and aDEL, hinting at a limited assistive contribution of the exoskeleton in tasks involving short and rapid movements. The results are consistent with a controller optimized for gravitational, rather than dynamic, compensation, which explains the exoskeleton's reduced effectiveness during dynamic tasks.

D. Carrying-load task

The outcomes of the carrying-load task are shown in Fig. 10 and Fig. 11. Fig. 10 (a) considers a representative subject to show both the right aDEL EMG signal and the temporal evolution of the vertical position of the lifted object during the subphases of the carrying-load task (see Subsection III-C) for each shelf height, as well as the trajectory of the object (i.e., position on the z-x plane) moved from the platform to the shelving unit during the carrying subphase of the same task. These trajectories are expressed in the reference system that is shown in Fig. 5 (a). For all the signals, the inter-subject mean has been included, and the time axis has been normalized. The release subphase may be further divided into a reaching stage lasting the first 20% of the whole time cycle on average, a releasing stage lasting from the 20% to the 60% of the whole time cycle on average, and a resting stage for the remaining 40% of the time cycle on average. Similarly, the pickup subphase can be divided into a reaching stage lasting the first 25% of the whole time cycle on average, a picking stage lasting from the 25% to the 70% of the whole time cycle on average, and a holding stage for the remaining 30% of the time cycle on average. Moreover, muscular activation increases on average as the height of the shelf on/from which to release/pick the object is greater. On the other hand, during the carrying subphase, the EMG signals oscillate around a mean value as the subjects move the object from the platform to the shelving while walking.

Fig. 10 (b) shows the distribution of the ITMV during the carrying-load task. When comparing the w. Exo and w.o. Exo conditions, for all three subphases of the task, no notable differences in the velocity suggest a uniform speed trend adopted among all participants while executing the task.

The distributions of ME during the carrying-load task for all subjects, divided by each subphase (i.e., pickup, carrying, release), are reported in Fig. 11. These results may be considered as intermediate between the isometric and the dynamic tasks in terms of the amount of both statistical significance and actual percentage reductions between the w. Exo and w.o. Exo conditions. Fig. 11 also shows some electromyographic imbalance between the left and the right sides of the aDEL in the release and the uTRA in the carrying subphases, due to a possible asymmetrical use of the exoskeleton, left to be naturally adjusted by each subject.

Statistically significant results concern the left (-45%, p=0.004) and right (-34.7%, p=0.035) mDEL and the right mPEC (-28.1%, p=0.004) in the Pickup phase, the left (-45.9%, p=0.026) and right (-45.8%, p=0.017) mDEL and the right mPEC (-45.8%, p=0.007) in the Carrying phase, the left aDEL (-15.1%, p=0.040) and the right mPEC (-20.3%, p=0.006) in the Release phase. These results confirm how the most relevant reductions in the ME are obtained when the subject is supported by the exoskeleton while performing isometric contractions for a longer time, in this case during the carrying subphase.

E. Qualitative feedback

Fig. 12 reports the scores of the NASA-TLX and RPE questionnaires related to both w. Exo and w.o. Exo conditions by means of a radar plot and a box plot, respectively. Since one questionnaire was provided to the subjects after completing all the tasks related to one condition (w. Exo or w.o. Exo) in series, the results refer to the median across all subjects, for all tasks of a single condition. More in detail, the scores related to the w. Exo condition are lower than those of the w.o. Exo condition for all the considered indexes; particularly,

This article has been accepted for publication in IEEE Transactions on Robotics. This is the author's version which has not been fully edited and content may change prior to final publication. Citation information: DOI 10.1109/TRO.2026.3666155

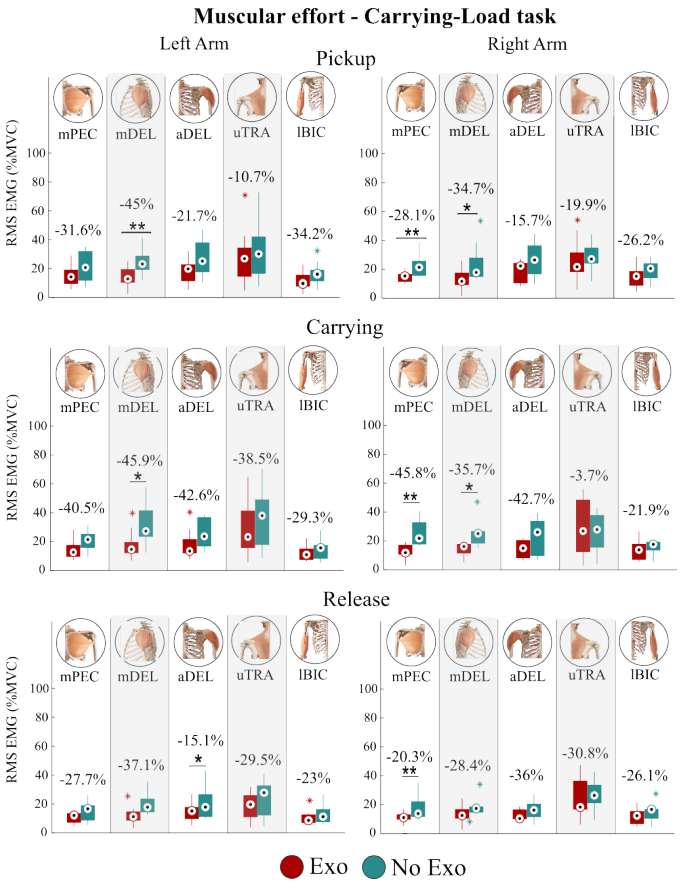

Fig. 11. RMS during the three main phases of the carrying-load task, with * and ** representing statistically significant comparisons with $p < .05$ and $p < .01$, respectively. Percentage differences in RMS between w. Exo and w.o. Exo conditions are reported.

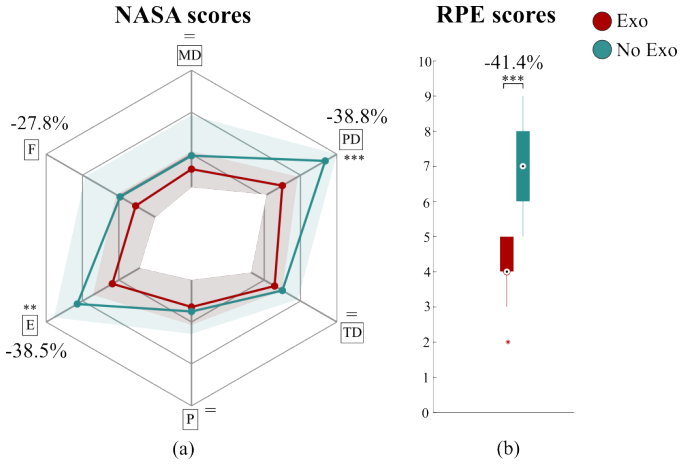

Fig. 12. Results of NASA-TLX and RPE questionnaires, with ** and *** representing statistically significant comparisons with $p < .01$ and $p < .001$, respectively. (a) The score distributions are depicted with a different polygon for each condition (i.e., w. Exo and w.o. Exo), as well as with the median highlighted through a thick line. The considered factors are mental demand (MD), physical demand (PD), temporal demand (TD), performance (P), effort (E), and frustration (F). (b) RPE scores. Moreover, the percentage differences in questionnaire scores between w. Exo and w.o. Exo conditions are reported. The = marks no reduction nor increase in the related index.

this difference is statistically significant for PD (-38.8%, p=0.0003) and E (-38.5%, p=0.0012). Additionally, the RPE score distribution to the w. Exo condition is significantly and consistently lower (-41.4%, p=0.00001) than that of the w.o. Exo condition. All these scores hint at a general trend of a subjective reduction of the perceived effort among subjects when assisted by Flexos. Although not statistically significant, the reduction in the F index (-27.8%, p=0.146) may suggest how subjects found the device comfortable to wear and easy to use, since extra care was taken in employing soft garments at the interfaces between the human body and Flexos' rigid parts. These results are mostly in line with other works from the literature [26], [39], confirming the crucial importance of an agreement between the subjectively perceived and the objectively assessed reduction in the user's physical effort.

F. Comparison in muscular activity

Results obtained from the experiments highlighted how the current Flexos system provides average muscular activity reductions - from 8% to 33%, from 7% to 32%, and from 22% to 32% for the isometric, dynamic, and carrying-load tasks, respectively - that are comparable with the ones of similar prototypes from the literature. This can be observed in Fig. 13, which reports the percentage variations in RMS for the presented study and related works through circles, whose center is the mean RMS reduction. These muscular reductions have been computed by averaging across body sides the percentage variations in RMS between the w.o. Exo and w. Exo conditions for each activity, load mass, and muscle.

The current system obtained muscular activity reductions that are comparable to passive devices. In fact, the majority of exoskeletons with similar assistive purposes, i.e., upper limbs for assisting shoulder flexion/extension, reached average reductions ranging from 3% to 40% [25], [26], [41]–[45]. The comparison with the studies of Pacifico et al. [42] and Grazi et al. [41] is appropriate when considering the respective levels of assistance. In this context, our findings indicate that the magnitudes of muscular effort reduction are comparable to those reported in their works. While greater reductions could reasonably be expected from a more powerful and fully active device, it is noteworthy that — despite Flexos being heavier than the passive device employed by Pacifico and Grazi — we achieved similar reductions in muscular activation at comparable assistive torque levels. This result can be attributed to the effective weight distribution of the proposed exoskeleton. Moreover, due to their passive actuation system, such exoskeletons do not allow for modifying in real-time the delivered torque, thus lacking versatility towards many adaptability, comfort, and safety features that active devices could implement. The results showed how the current system obtained reductions in muscular activity comparable to those of passive devices, with the additional feature of being an active device.

For comparison with active devices, in [40] an active exoskeleton was realized, obtaining reductions by 32% (aDEL), 57% (mDEL), and 45% (lBIC) for the static task and by 25% (aDEL), 50% (mDEL) - with lBIC showing a non-significant reduction - for the dynamic task. However, the exoskeleton had Bowden cable actuation, thus being still not portable - as the

This article has been accepted for publication in IEEE Transactions on Robotics. This is the author's version which has not been fully edited and content may change prior to final publication. Citation information: DOI 10.1109/TRO.2026.3666155

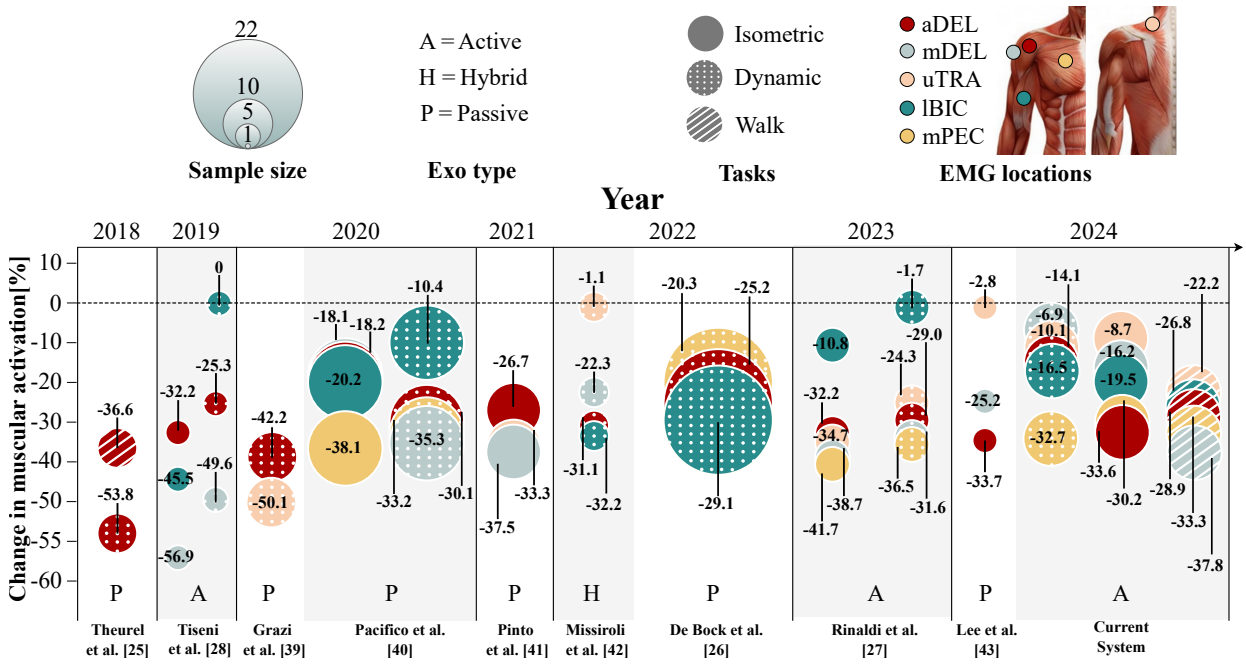

Fig. 13. Related works employing similar exoskeletons supporting the shoulder flexion. For each activity, load mass, and muscle, the percentage variations in RMS between the w.o. Exo and w. Exo conditions are averaged across the body sides. The resulting variations in muscular effort are reported with circles, whose center is the mean RMS reduction, whose radius is connected with the sample size, whose color is the muscle, and whose texture is the activity. Mean RMS reductions are textually reported on the related circle. Acronyms: aDEL - anterior deltoid; mDEL - medial deltoid; uTRA - upper trapezius; lBIC: biceps brachii; mPEC: pectoralis major.

TABLE VI
RELEVANT FEATURES FROM RELATED WORKS, REPORTED FOR COMPARISONS AMONG PROTOTYPES.

	Theurel et al. [25]	**Tiseni et al.** [40]	**Grazi et al.** [41]	**Pacifico et al.** [42]	**Pinto et al.** [43]	**Missiroli et al.** [44]	**De Bock et al.** [26]	**Rinaldi et al.** [27]	**Lee et al.** [45]	**Current System**
Mass (kg)	9	2.45	5	3.5	3	6.4	3.8	4.8	1.9	8
Actuation Type	Passive	Active	Passive	Passive	Passive	Hybrid	Passive	Active	Passive	Active
Max Torque *Absolute* (N m)	assistance at EE up to 135° (flex.)	20	6	5.5	ND	ND	3	9	5	9
Max. Torque *Experiments* (N m)	assistance at EE 9 kg (Males) 5 kg (Females) up to 90°	2.5	4.58 (Low) 5.38 (Medium) 5.85 (High)	4	ND	ND	3	5	2.5	5
Target Load Mass (kg)	15 (Males) 8 (Females)	0	0	0	0	1.5	5 (static tasks) 10 (dynamic tasks)	2	1.2 (drilling task) 5 (lifting task)	3, 5 (static task) 3, 5 (dynamic tasks) 3 (carrying-load task)
Body Side	Both	Right	Both	Both	Both	Both	Both	Right	Both	Both
Sample Size	8	5	10	15	12	6	22	7	5	12

current system - which is a relevant feature for occupational devices. Additionally, the preliminary study conducted with the previous version of Flexos [27] led to reductions ranging from 11% to 42% and from 2% to 37% for the static and the dynamic task, respectively. These results differ from the current ones, mainly due to the bilaterality of the current Flexos instead of the unilaterality of the old one, a feature that necessarily contributed to a limited increase in the device's weight; besides, the previous experiments were characterized by both a lower sample size and thoroughly different (and simpler) tasks.

Other relevant features from related works are reported in Table VI for further comparisons.

The mechanical design has made Flexos a valid and advantageous alternative to other prototypes for several reasons: the wearability is increased by the soft garments between the human body and Flexos' rigid parts; the human shoulder ROM is extensively covered in the DOFs of both flexion/extension and internal/external rotation; the adaptability to the different wearer's width sizes has been enhanced through the modularity of the flexible link (see Figure 2(a)); a similar assistance level compared to passive exoskeletons, together with a higher perceived comfort thanks to Flexos active nature; an intrinsic safety ensured by the SEA and a high interaction transparency thanks to the torque controller; and an effective weight distribution attenuating the higher heaviness of the proposed active exoskeleton, thus allowing for comparable reductions of the objectively and subjectively assessed muscular efforts with

respect to passive devices.

G. Limitations

Despite the promising results, this study highlighted some issues, starting from the design of the exoskeleton that is mostly indicated for wearers of $1.68\,\mathrm{m}$ of minimum height. The modularity of the flexible link connecting the back side of the exoskeleton with the arms allows the device to fit different width sizes; however, the user's height still provides an exclusion criteria to better exploit the advantages of this device.

Moreover, all the SEA torque could not be used due to the insufficient stiffness in the flexible link, which is 3D-printed, resulting in torsional displacements under load. Additionally, the SEAs weight could impact the effectiveness of the device itself: Flexos torque-to-weight ratio now stands at $0.66\,\mathrm{Nm/kg}$, which might be underwhelming if compared to the most commonly employed passive solutions. Nonetheless, the device's active features manage to compensate for the low torque-to-weight ratio by including, for example, Flexos' capability of inhibiting its assistance when the user is bending to collect an object from the ground. In this study, this feature was used during the experiments only to promote the user's comfort, and a future study will investigate the impact of the two assistance modes (i.e., with and without torque modulation). Although a more versatile implementation of an active system would be the estimation of different payloads to modulate the exoskeleton assistance accordingly, Flexos still offers a significant advantage by modulating its support based on the user's movements (i.e., the bending). On the other hand, the introduction of a feedforward term has allowed the reduction of delay from $100\,\mathrm{ms}$ to $45\,\mathrm{ms}$, but the possible impact of this improvement on the system performance in terms of tracking accuracy, transparency, and EMG reductions needs to be proved by further future experiments.

Regarding possible side-effects of Flexos usage, the electromyographic activity of the left bicep, which is not directly assisted by the exoskeleton but still involved in the shoulder flexion/extension, proved to undergo no particular side effects, since reductions were provided in the w. Exo condition. However, as previously highlighted in Subsections IV-C and IV-D, some imbalances in the ME results hint at a possible asymmetrical usage of the device, as the wearer is left with freedom of adjustment once Flexos is worn. Additionally, Flexos is designed to discharge the load towards the lumbar area: possible side effects on the legs were not investigated in this work, since the focus was kept on the upper body.

Moreover, we want to note that the accuracy of the shoulder flexion angle estimation is directly related to the BNO055 IMU sensor. As reported by Shenoy et al. [46]; in the worst case, the RMSE error of the angle estimation is of $7.5\,^\circ$. Thus, it may have led to the execution of an isometric task at $80\,^\circ$ in the worst case, at some moments of the experiment.

Lastly, we acknowledge that the experimental protocol includes occupational tasks that are not fully representative of those found in typical workplace scenarios. Given that this study is an in-lab assessment, with limitations regarding the usage of common spaces, the duration of tasks was kept reduced compared to the $8\,\mathrm{hours}$ of a standard work shift. Moreover, the designed tasks feature several isometric motions, with the shoulders flexed at $90\,^\circ$ in correspondence of the maximum gravity effect. Although not fully reflecting real use cases, they provide an ideal test for the maximum assistive effect of the exoskeleton in the worst case. However, it should be noted how a real-job activity features a set of complex gestures and motions, which would require a more sophisticated investigation on the device and its ability to reduce the user's effort [41]. In this work, the primary intention was to create boundary cases in which shoulder assistance is critically needed to demonstrate the concept behind the Flexos exoskeleton.

V. Conclusion

In conclusion, this work demonstrated how the Flexos exoskeleton provided an assistive benefit during the execution of repetitive shoulder flexion/extension movements to lift, carry, and shelve objects that are non-excessively heavy. This evaluation framework was designed to feature occupational tasks that took place inside a research laboratory, with a device that is still a prototype, and on a limited number of healthy subjects. We acknowledge all the limitations of this extended study and we intend to address them in future works.

Nonetheless, the results are promising: despite its simple, under-actuated design, Flexos helps the user relieve the effort related to the shoulder complex muscles in almost all cases. If the reduction of an index is not supported by statistical significance, the device does not worsen the subject's performance. On the other hand, in the few cases where Flexos usage provides worsening results, the increasing of an index is minimal and never statistically significant, even though further studies to exclude any possible side effects on the lower body are needed. Particularly, Flexos enhances the subject's performance, especially in the motor actions that involved to perform isometric contractions for a longer time, such as carrying a load with shoulder flexed at $90\,^\circ$ on the sagittal plane.

The exposed concept represents another step towards a larger adoption of occupational exoskeletons in the daily work routine of industrial operators, concurring in the prevention of work-related musculoskeletal disorders for a healthier and safer workplace where humans are assisted but not replaced by robots.

Acknowledgements

This work was supported by the BRIEF project "Biorobotics Research and Innovation Engineering Facilities" (project identification code IR0000036) funded under the National Recovery and Resilience Plan (NRRP), Mission 4: "Istruzione e Ricerca", Component 2: "Dalla ricerca all'impresa", Investment 3.1: "Fondo per la realizzazione di un sistema integrato di infrastrutture di ricerca e innovazione", CUP: J13C22000400007, funded by the European Union - NextGenerationEU.

REFERENCES

[1] J. de Kok, P. Vroonhof, J. Snijders, and G. R. et al., "Work-related msds: prevalence, costs and demographics in the eu," European Agency for Safety and Health at Work, Tech. Rep., 2019.

[2] F. Yang, N. Di, W.-w. Guo, W.-b. Ding, N. Jia, H. Zhang, D. Li, D. Wang, R. Wang, D. Zhang *et al.*, "The prevalence and risk factors of work related musculoskeletal disorders among electronics manufacturing workers: a cross-sectional analytical study in china," *BMC Public Health*, vol. 23, no. 1, p. 10, 2023. [Online]. Available: https://doi.org/10.1186/s12889-022-14952-6

[3] K. Huysamen, T. Bosch, M. de Looze, K. S. Stadler, E. Graf, and L. W. O'Sullivan, "Evaluation of a passive exoskeleton for static upper limb activities," *Applied Ergonomics*, vol. 70, pp. 148–155, 2018. [Online]. Available: https://doi.org/10.1016/j.apergo.2018.02.009

[4] M. A. Gull, S. Bai, and T. Bak, "A review on design of upper limb exoskeletons," *Robotics*, vol. 9, no. 1, p. 16, 2020. [Online]. Available: https://doi.org/10.3390/robotics9010016

[5] S. Crea, P. Beckerle, M. De Looze, K. De Pauw, L. Grazi, T. Kermavnar, J. Masood, L. W. O'Sullivan, I. Pacifico, C. Rodriguez-Guerrero *et al.*, "Occupational exoskeletons: A roadmap toward large-scale adoption. methodology and challenges of bringing exoskeletons to workplaces," *Wearable Technologies*, vol. 2, p. e11, 2021. [Online]. Available: https://doi.org/10.1017/wtc.2021.11

[6] C. Weckenborg, C. Thies, and T. S. Spengler, "Harmonizing ergonomics and economics of assembly lines using collaborative robots and exoskeletons," *Journal of Manufacturing Systems*, vol. 62, pp. 681–702, 2022. [Online]. Available: https://doi.org/10.1016/j.jmsy.2022.02.005

[7] S. Christensen, S. Bai, S. Rafique, M. Isaksson, L. O'Sullivan, V. Power, and G. S. Virk, "Axo-suit-a modular full-body exoskeleton for physical assistance," in *IFToMM Symposium on Mechanism Design for Robotics*. Springer, 2018, pp. 443–450. [Online]. Available: https://doi.org/10.1007/978-3-030-00365-4_52

[8] A.-M. Georgarakis, M. Xiloyannis, P. Wolf, and R. Riener, "A textile exomuscle that assists the shoulder during functional movements for everyday life," *Nature Machine Intelligence*, vol. 4, no. 6, pp. 574–582, 2022. [Online]. Available: https://doi.org/10.1038/s42256-022-00495-3

[9] C. M. Thalman, Q. P. Lam, P. H. Nguyen, S. Sridar, and P. Polygerinos, "A novel soft elbow exosuit to supplement bicep lifting capacity," in *2018 IEEE/RSJ International Conference on Intelligent Robots and Systems (IROS)*, 2018, pp. 6965–6971.

[10] D. Chiaradia, L. Tiseni, M. Xiloyannis, M. Solazzi, L. Masia, and A. Frisoli, "An assistive soft wrist exosuit for flexion movements with an ergonomic reinforced glove," *Frontiers in Robotics and AI*, vol. 7, p. 595862, 2021. [Online]. Available: https://doi.org/10.3389/frobt.2020.595862

[11] A. Voilqué, J. Masood, J. Fauroux, L. Sabourin, and O. Guezet, "Industrial exoskeleton technology: classification, structural analysis, and structural complexity indicator," in *2019 Wearable Robotics Association Conference (WearRAcon)*. IEEE, 2019, pp. 13–20. [Online]. Available: https::/www.doi.org/10.1109/WEARRACON.2019.8719395

[12] "Mate by comau," https://mate.comau.com/, Last accessed on 2023-02-04.

[13] "Skelex," https://www.skelex.com/, Last accessed on 2023-02-04.

[14] "Max by suit x," https://www.suitx.com/, Last accessed on 2023-02-04.

[15] "Ergosquelettes," https://gobio-robot.com/, Last accessed on 2023-02-04.

[16] J. Sänger, Z. Yao, T. Schubert, A. Wolf, C. Molz, J. Miehling, S. Wartzack, T. Gwosch, S. Matthiesen, and R. Weidner, "Evaluation of active shoulder exoskeleton support to deduce application-oriented optimization potentials for overhead work," *Applied Sciences*, vol. 12, no. 21, p. 10805, 2022.

[17] G. A. Pratt and M. M. Williamson, "Series elastic actuators," in *Proceedings 1995 IEEE/RSJ International Conference on Intelligent Robots and Systems. Human Robot Interaction and Cooperative Robots*, vol. 1. IEEE, 1995, pp. 399–406. [Online]. Available: https://doi.org/10.1109/IROS.1995.525827

[18] C. Camardella, M. Barsotti, D. Buongiorno, A. Frisoli, and V. Bevilacqua, "Towards online myoelectric control based on muscle synergies-to-force mapping for robotic applications," *Neurocomputing*, vol. 452, pp. 768–778, 2021. [Online]. Available: https://doi.org/10.1016/j.neucom.2020.08.081

[19] A. Ebrahimi, "Stuttgart exo-jacket: An exoskeleton for industrial upper body applications," in *2017 10th International Conference on Human System Interactions (HSI)*. IEEE, 2017, pp. 258–263. [Online]. Available: https://doi.org/10.1109/HSI.2017.8005042

[20] P. Maurice, J. Čamernik, D. Gorjan, B. Schirrmeister, J. Bornmann, L. Tagliapietra, C. Latella, D. Pucci, L. Fritzsche, S. Ivaldi *et al.*, "Objective and subjective effects of a passive exoskeleton on overhead work," *IEEE Transactions on Neural Systems and Rehabilitation Engineering*, vol. 28, no. 1, pp. 152–164, 2019. [Online]. Available: https://doi.org/10.1109/TNSRE.2019.2945368

[21] A. Blanco, J. M. Catalán, D. Martínez-Pascual, J. V. García-Pérez, and N. García-Aracil, "The effect of an active upper-limb exoskeleton on metabolic parameters and muscle activity during a repetitive industrial task," *IEEE Access*, vol. 10, pp. 16 479–16 488, 2022. [Online]. Available: https://doi.org/10.1109/ACCESS.2022.3150104

[22] L. Grazi, E. Trigili, N. Caloi, G. Ramella, F. Giovacchini, N. Vitiello, and S. Crea, "Kinematics-based adaptive assistance of a semi-passive upper-limb exoskeleton for workers in static and dynamic tasks," *IEEE Robotics and Automation Letters*, vol. 7, no. 4, pp. 8675–8682, 2022. [Online]. Available: https://doi.org/10.1109/LRA.2022.3188402

[23] Y. M. Zhou, C. Hohimer, T. Proietti, C. T. O'Neill, and C. J. Walsh, "Kinematics-based control of an inflatable soft wearable robot for assisting the shoulder of industrial workers," *IEEE Robotics and Automation Letters*, vol. 6, no. 2, pp. 2155–2162, 2021. [Online]. Available: https://doi.org/10.1109/LRA.2021.3061365

[24] A. Coccia, E. M. Capodaglio, F. Amitrano, V. Gabba, M. Panigazzi, G. Pagano, and G. D'Addio, "Biomechanical effects of using a passive exoskeleton for the upper limb in industrial manufacturing activities: A pilot study," *Sensors*, vol. 24, no. 5, 2024. [Online]. Available: https://www.mdpi.com/1424-8220/24/5/1445

[25] J. Theurel, K. Desbrosses, T. Roux, and A. Savescu, "Physiological consequences of using an upper limb exoskeleton during manual handling tasks," *Applied ergonomics*, vol. 67, pp. 211–217, 2018. [Online]. Available: https://doi.org/10.1016/j.apergo.2017.10.008

[26] S. De Bock, M. Rossini, D. Lefeber, C. Rodriguez-Guerrero, J. Geeroms, R. Meeusen, and K. De Pauw, "An occupational shoulder exoskeleton reduces muscle activity and fatigue during overhead work," *IEEE Transactions on Biomedical Engineering*, vol. 69, no. 10, pp. 3008–3020, 2022. [Online]. Available: https://www.doi.org/10.1109/TBME.2022.3159094

[27] G. Rinaldi, L. Tiseni, M. Xiloyannis, L. Masia, A. Frisoli, and D. Chiaradia, "Flexos: A portable, sea-based shoulder exoskeleton with hyper-redundant kinematics for weight lifting assistance," in *2023 IEEE World Haptics Conference (WHC)*. IEEE, 2023, pp. 252–258. [Online]. Available: https://www.doi.org/10.1109/WHC56415.2023.10224485

[28] L. Tiseni, G. Rinaldi, D. Chiaradia, and A. Frisoli, "Design and control of a linear springs-based rotary series elastic actuator for portable assistive exoskeletons," in *2021 30th IEEE International Conference on Robot & Human Interactive Communication (RO-MAN)*, 2021, pp. 434–439. [Online]. Available: https://doi.org/10.1109/RO-MAN50785.2021.9515444

[29] M. J. Kim, A. Werner, F. C. Loeffl, and C. Ott, "Enhancing joint torque control of series elastic actuators with physical damping," in *2017 IEEE International Conference on Robotics and Automation (ICRA)*, 2017, pp. 1227–1234.

[30] W. T. Dempster and G. R. Gaughran, "Properties of body segments based on size and weight," *American journal of anatomy*, vol. 120, no. 1, pp. 33–54, 1967.

[31] M. Żuk, M. Wojtków, M. Popek, J. Mazur, and K. Bulińska, "Three-dimensional gait analysis using a virtual reality tracking system," *Measurement*, vol. 188, p. 110627, 2022. [Online]. Available: https://doi.org/10.1016/j.measurement.2021.110627

[32] "The seniam project (surface electromyography for the non- invasive assessment of muscles," http://www.seniam.org/, Last accessed on 2023-02-04.

[33] R. Merletti and D. Farina, *Myoelectric Manifestations of Muscle Fatigue*. John Wiley & Sons, Ltd, 2006. [Online]. Available: https://onlinelibrary.wiley.com/doi/abs/10.1002/9780471740360.ebs1427

[34] E. Rashedi, S. Kim, M. A. Nussbaum, and M. J. Agnew, "Ergonomic evaluation of a wearable assistive device for overhead work," *Ergonomics*, vol. 57, no. 12, pp. 1864–1874, 2014. [Online]. Available: https://doi.org/10.1080/00140139.2014.952682

[35] S. G. Hart, "Nasa-task load index (nasa-tlx); 20 years later," *Proceedings of the Human Factors and Ergonomics Society Annual Meeting*, vol. 50, no. 9, pp. 904–908, 2006. [Online]. Available: https://doi.org/10.1177/154193120605000909

[36] G. Borg, "Psychophysical scaling with applications in physical work and the perception of exertion," *Scandinavian Journal of Work, Environment & Health*, vol. 16, pp. 55–58, 2024/04/10/ 1990. [Online]. Available: http://www.jstor.org/stable/40965845

[37] D. C. Boone and S. P. Azen, "Normal range of motion of joints in male subjects." *JBJS*, vol. 61, no. 5, pp. 756–759, 1979.

[38] G. Wu, F. van der Helm, H. D. Veeger, M. Makhsous, P. Van Roy, C. Anglin, J. Nagels, A. R. Karduna, K. McQuade, X. Wang, F. W. Werner, and B. Buchholz, "Isb recommendation on definitions of joint coordinate systems of various joints for the reporting of human joint motion–part ii: shoulder, elbow, wrist and hand." *Journal of Biomechanics*, vol. 38,5, pp. 981–992, 2005. [Online]. Available: https://doi.org/10.1016/j.jbiomech.2004.05.042

[39] K. Langlois, D. Rodriguez-Cianca, B. Serrien, J. De Winter, T. Verstraten, C. Rodriguez-Guerrero, B. Vanderborght, and D. Lefeber, "Investigating the effects of strapping pressure on human-robot interface dynamics using a soft robotic cuff," *IEEE Transactions on Medical Robotics and Bionics*, vol. 3, no. 1, pp. 146–155, 2021.

[40] L. Tiseni, M. Xiloyannis, D. Chiaradia, N. Lotti, M. Solazzi, H. Van der Kooij, A. Frisoli, and L. Masia, "On the edge between soft and rigid: an assistive shoulder exoskeleton with hyper-redundant kinematics," in *2019 IEEE 16th International Conference on Rehabilitation Robotics (ICORR)*. IEEE, 2019, pp. 618–624. [Online]. Available: https://www.doi.org/10.1109/ICORR.2019.8779546

[41] L. Grazi, E. Trigili, G. Proface, F. Giovacchini, S. Crea, and N. Vitiello, "Design and experimental evaluation of a semi-passive upper-limb exoskeleton for workers with motorized tuning of assistance," *IEEE Transactions on Neural Systems and Rehabilitation Engineering*, vol. 28, no. 10, pp. 2276–2285, 2020. [Online]. Available: https://doi.org/10.1016/10.1109/TNSRE.2020.3014408

[42] I. Pacifico, A. Scano, E. Guanziroli, M. Moise, L. Morelli, A. Chiavenna, D. Romo, S. Spada, G. Colombina, F. Molteni *et al.*, "An experimental evaluation of the proto-mate: a novel ergonomic upper-limb exoskeleton to reduce workers' physical strain," *IEEE Robotics & Automation Magazine*, vol. 27, no. 1, pp. 54–65, 2020. [Online]. Available: https::/www.doi.org/10.1109/MRA.2019.2954105

[43] T. Pinto, F. dos Anjos, T. Vieira, G. L. Cerone, R. Sessa, F. Caruso, G. Caragnano, F. S. Violante, and M. Gazzoni, "The effect of passive exoskeleton on shoulder muscles activity during different static tasks," in *8th European Medical and Biological Engineering Conference*, T. Jarm, A. Cvetkoska, S. Mahnič-Kalamiza, and D. Miklavcic, Eds. Cham: Springer International Publishing, 2021, pp. 1087–1091. [Online]. Available: https://doi.org/10.1007/978-3-030-64610-3_122

[44] F. Missiroli, N. Lotti, E. Tricomi, C. Bokranz, R. Alicea, M. Xiloyannis, J. Krzywinski, S. Crea, N. Vitiello, and L. Masia, "Rigid, soft, passive, and active: A hybrid occupational exoskeleton for bimanual multijoint assistance," *IEEE Robotics and Automation Letters*, vol. 7, no. 2, pp. 2557–2564, 2022. [Online]. Available: https://doi.org/10.1109/LRA.2022.3142447

[45] H.-H. Lee, K.-T. Yoon, H.-H. Lim, W.-K. Lee, J.-H. Jung, S.-B. Kim, and Y.-M. Choi, "A novel passive shoulder exoskeleton using link chains and magnetic spring joints," *IEEE Transactions on Neural Systems and Rehabilitation Engineering*, vol. 32, pp. 708–717, 2024. [Online]. Available: https://www.doi.org/10.1109/TNSRE.2024.3359658

[46] P. Shenoy, A. Gupta, and V. S.K.M., "Design and validation of an imu based full hand kinematic measurement system," *IEEE Access*, vol. 10, pp. 93 812–93 830, 2022.

G. Rinaldi received the B.Sc. degree in Electrical Engineering and the M.Sc. degree with honors in Robotics and Automation Engineering from the University of Pisa, Italy, in 2017 and 2022, respectively. He received his Ph.D. in Emerging Digital Technologies at the Institute of Mechanical Intelligence of Scuola Superiore Sant'Anna in Pisa, Italy, in 2025. His research is mainly centered on human-robot interaction, particularly in the field of occupational exoskeletons for upper limbs.

V. Suglia is a collaborator of the Bioengineering Laboratory at the Polytechnic University of Bari, Italy. He received the B.Sc. degree in computer science and automation Engineering, the M.Sc. degree in automation Engineering (both with honors), and his Ph.D. in electrical and information engineering from the Polytechnic University of Bari, Italy, in 2018, 2021, and 2025 respectively. His main research interests include human-robot interaction, biomedical signals, virtual reality, and artificial intelligence.

L. Tiseni is Chief Technology Officer at Next Generation Robotics Srl. He received his M.Sc. degree in mechanical engineering with honors from the University of Pisa in 2018, and his Ph.D. with honors in Emerging Digital Technologies from the Institute of Mechanical Intelligence of Sant'Anna School of Advanced Studies in Pisa, Italy, in 2023. His main research topics are human-robot interaction and robotic train inspection.

C. Camardella is a researcher in the Perceptual Robotics laboratory in the Mechanical Intelligence Institute of Scuola Superiore Sant'Anna. He received the Master's degree in control theory and automation engineering from the Polytechnic of Bari in 2017, and a PhD in Emerging Digital Technologies from Scuola Superiore Sant'Anna in 2021. He is currently working on distributed haptic systems, predictive systems, and robotic platforms in the rehabilitation robotics field, and immersive VR serious games. His interests cover machine learning and artificial intelligence, robotic exoskeletons and control strategies, muscle synergies, and serious game optimization.

M. Xiloyannis received the bachelor's degree in biomedical engineering from the University of Pisa, Italy, and an M.Sc. degree in neurotechnology from Imperial College London, London, U.K., in 2014. He then completed a PhD in Robotics at NTU Singapore, under the supervision of Prof. Lorenzo Masia, on the design and assessment of soft wearable robots to support people with mobility disorders. He is currently the Chief Technology Officer at Akina AG, Zurich, Switzerland.

This article has been accepted for publication in IEEE Transactions on Robotics. This is the author's version which has not been fully edited and content may change prior to final publication. Citation information: DOI 10.1109/TRO.2026.3666155

L. Masia (Senior Member, IEEE) received his master in mechanical engineering at "Sapienza" University of Rome in 2003 and the Ph.D. degree from the University of Padua, Italy, in 2007. He is currently Full Professor of "Intelligent Bio-Robotic Systems" at the Technische Universität München (TUM), Munich, Germany, leading the Assistive Robotics and Interactive ExoSuits (ARIES) Lab, and he serves as Executive Director of the Munich Institute for Robotics and Machine Intelligence (MIRMI). Before his appointment at TUM he was Full Professor at Heidelberg University, Heidelberg, Germany. He spent two years at the Mechanical Engineering Department, Massachusetts Institute of Technology. He was an Assistant Professor with the School of Mechanical & Aerospace Engineering, Nanyang Technological University, Singapore, and an Associate Professor of Biodesign with the University of Twente, The Netherlands. Professor Masia is recipient of five best paper awards in IEEE RAS and EMBS conferences.

D. Buongiorno is an assistant professor in Bioengineering at the Department of Electrical and Information Engineering at the Polytechnic University of Bari, where he teaches biomedical instrumentation. He earned his Bachelor's and Master's degrees in control system engineering from the Polytechnic University of Bari in 2011 and 2014, respectively. In 2017, he obtained his PhD in Emerging Digital Technologies from the Sant'Anna School of Advanced Studies in Pisa. Until July 2022, he worked as a postdoctoral research fellow in the field of electronic and computer bioengineering. His research activity focuses on intelligent systems for diagnosis and therapy.

V. Bevilacqua Vitoantonio Bevilacqua is Full Professor of bioengineering with the Electrical and Information Engineering Department, Polytechnic University of Bari, where he is the head of the Industrial Informatics Laboratory and coordinator of the master's degree in medical systems engineering. In September 2019, he joined as an affiliate Professor at the BioRobotics Institute, Scuola Superiore Sant'Anna di Pisa. Since 1996, he has been working and investigating in the fields of computer vision and image processing, bioengineering, human-machine interaction based on machine learning, and soft computing techniques. He is also CEO of Apulian Bioengineering s.r.l., a spin-off company of the Polytechnic University of Bari.

A. Frisoli (Senior Member, IEEE) is a Full Professor of mechanical engineering and robotics with Scuola Superiore Sant'Anna (SSSA), Italy, where he leads the Human-Robot Interaction area of the Institute of Mechanical Intelligence. He is currently responsible for the SSSA macro node of the Artes4.0 competence center on collaborative robotics. He is an Associate Editor of IEEE Robotics and Automation Magazine and covers several scientific and editorial roles in scientific societies (Eurohaptics and ICORR), international conferences, and journals. His research interests are in the area of collaborative, rehabilitative, and wearable robotics, exoskeletons, multimodal interaction, teleoperation, and haptics. He is very active in technology transfer and open innovation and has been the Co-Founder of two spin-offs (Wearable Robotics srl and Next Generation Robotics srl).

D. Chiaradia is Assistant Professor of mechanical engineering focusing on robotics at Sant'Anna School of Advanced Studies, Pisa, Italy. He leads the group developing flexible and portable exoskeletons, and soft exosuits in the Human Robot Interaction (HRI) research area. He received the B.Sc and M.Sc. degrees with honors in control theory and automation engineering from the Polytechnic University of Bari, Italy, in 2011 and 2014, respectively. He obtained the Ph.D. degree in emerging digital technologies, perceptual robotics curriculum, at Scuola Superiore Sant'Anna in 2018. His current research interests include physical human-robot interaction, occupational exoskeletons and soft exosuits for assistance and rehabilitation, mechanical design and control of flexible joints, and haptic interfaces. He is one of the founding members of Next Generation Robotics, a Sant'Anna spin-off operating in the collaborative and industrial robotics domain.